

Heparan sulfate proteoglycans regulate autophagy in *Drosophila*

Claire E. Reynolds-Peterson[†], Na Zhao[†], Jie Xu, Taryn M. Serman, Jieli Xu, and Scott B. Selleck

Department of Biochemistry and Molecular Biology, The Pennsylvania State University, University Park, PA, USA

ABSTRACT

Heparan sulfate-modified proteoglycans (HSPGs) are important regulators of signaling and molecular recognition at the cell surface and in the extracellular space. Disruption of HSPG core proteins, HS-synthesis, or HS-degradation can have profound effects on growth, patterning, and cell survival. The *Drosophila* neuromuscular junction provides a tractable model for understanding the activities of HSPGs at a synapse that displays developmental and activity-dependent plasticity. Muscle cell-specific knockdown of HS biosynthesis disrupted the organization of a specialized postsynaptic membrane, the subsynaptic reticulum (SSR), and affected the number and morphology of mitochondria. We provide evidence that these changes result from a dysregulation of macroautophagy (hereafter referred to as autophagy). Cellular and molecular markers of autophagy are all consistent with an increase in the levels of autophagy in the absence of normal HS-chain biosynthesis and modification. HS production is also required for normal levels of autophagy in the fat body, the central energy storage and nutritional sensing organ in *Drosophila*. Genetic mosaic analysis indicates that HS-dependent regulation of autophagy occurs non-cell autonomously, consistent with HSPGs influencing this cellular process via signaling in the extracellular space. These findings demonstrate that HS biosynthesis has important regulatory effects on autophagy and that autophagy is critical for normal assembly of postsynaptic membrane specializations.

ARTICLE HISTORY

Received 22 June 2015
Revised 22 February 2017
Accepted 6 March 2017

KEYWORDS



autophagy; *Drosophila*;
heparan sulfate
proteoglycan; mitochondria;
subs synaptic reticulum

Introduction


Heparan sulfate-modified proteins are ubiquitous components of the cell surface and extracellular matrix. These highly sulfated macromolecules play crucial roles in regulating developmental signaling pathways, including WNT/Wingless, Hedgehog, BMP/Bone Morphogenetic Protein families, TGFB/Transforming Growth Factor- β , and FGF/Fibroblast Growth Factors in a myriad of systems.^{1–5} HSPGs have diverse biological functions, affecting assembly of growth factor-receptor complexes, the stability of growth factors in the matrix, production of morphogen gradients, and endocytic clearance of cell surface-bound ligands. Disruption of individual HSPG core proteins, HS-biosynthesis or modification, HS-desulfation or degradation can have profound effects on morphogenesis, lipid catabolism, and cell survival.^{6,7}

We have been using the *Drosophila* neuromuscular junction to investigate the molecular and cellular functions of HSPGs during synapse development. HSPGs are concentrated at the neuromuscular junction (NMJ) and play a critical role in signaling events that coordinate motoneuron and muscle cell interactions. The HSPGs Sdc (syndecan) and dlp (dally-like) influence the signaling of the protein tyrosine phosphatase Lar (leukocyte-antigen-related-like) at the presynaptic-terminal, affecting both terminal growth

and active zone assembly.^{8,9} The protein trol (terribly reduced optic lobes), a secreted HSPG, affects both motoneuron terminal outgrowth and the elaboration of a postsynaptic specialization, the subsynaptic reticulum (SSR), apparently by governing wg/Wnt signaling at the synapse.¹⁰ Our earlier work examining the effects of HS biosynthesis on NMJ structure reveals the critical requirement for HSPGs in both the pre- and postsynaptic cells, consistent with the aforementioned studies examining the functions of individual HSPGs and their molecular partners. In particular, we note several striking effects on the cellular organization of the postsynaptic cell, namely disorganization of the SSR and loss of mitochondria.¹¹ The work described here reveals the cellular basis for these phenotypes, showing that loss of HSPGs produces activation of autophagy in the muscle cell. The function of HSPGs in suppressing autophagy is not limited to muscle. A mutation affecting HS polymer synthesis or RNA interference of genes required for either HS synthesis or sulfation produced elevated levels of autophagy in the fat body, an organ critical for energy sensing and storage. These findings suggest that HSPG-mediated signaling can affect autophagy in multiple cell types and provide a general mechanism for affecting the levels of this critical cellular process.

CONTACT Scott B. Selleck  sbs24@psu.edu  Department of Biochemistry and Molecular Biology, The Pennsylvania State University, University Park, PA 16802, USA.

[†]Contributed equally to this work.

 Supplemental data for this article can be accessed on the [publisher's website](#).

© 2017 Claire E. Reynolds-Peterson, Na Zhao, Jie Xu, Taryn M. Serman, Jieli Xu, and Scott B. Selleck. Published with license by Taylor & Francis.

This is an Open Access article distributed under the terms of the Creative Commons Attribution-Non-Commercial License (<http://creativecommons.org/licenses/by-nc/3.0/>), which permits unrestricted non-commercial use, distribution, and reproduction in any medium, provided the original work is properly cited. The moral rights of the named author(s) have been asserted.

projections (Fig. 1 C). Each synaptic connection consists of numerous boutons, defined as a single bud of the axonal terminal (red) and the surrounding subsynaptic membrane compartments (green) (Fig. 1 D). The intense GFP signal seen at the NMJ surrounding the motoneuron bouton is a function of the complex and dense membrane assembly of the SSR, visualized with mCD8-GFP.

The SSR is a highly ordered postsynaptic membrane structure where cytoskeletal, neurotransmitter receptor, and signaling molecules are spatially localized.^{19,20} During development, the SSR expands proportionally as the muscle cell grows. The SSR also shows use-dependent plasticity, with expansion occurring as a

function of synaptic activity.²¹ Genes required for SSR elaboration such as *Syx18* and *Akt1* are also critical for the physiological properties of this synapse, independent of the changes in neurotransmitter receptors.^{22,23} Therefore, assembly and structure of the SSR is a critical determinant of NMJ function. Ultrastructural changes of the NMJ in response to reduction of *sfl* or *ttv* function were assessed by transmission electron microscopy (TEM) of motoneuron terminals and the underlying postsynaptic specializations (Fig. 2, A to C, Ai to Ci). Reduction of either *sfl* or *ttv* function with muscle-directed RNAi expanded the spaces between membrane layers of the SSR. This SSR structural

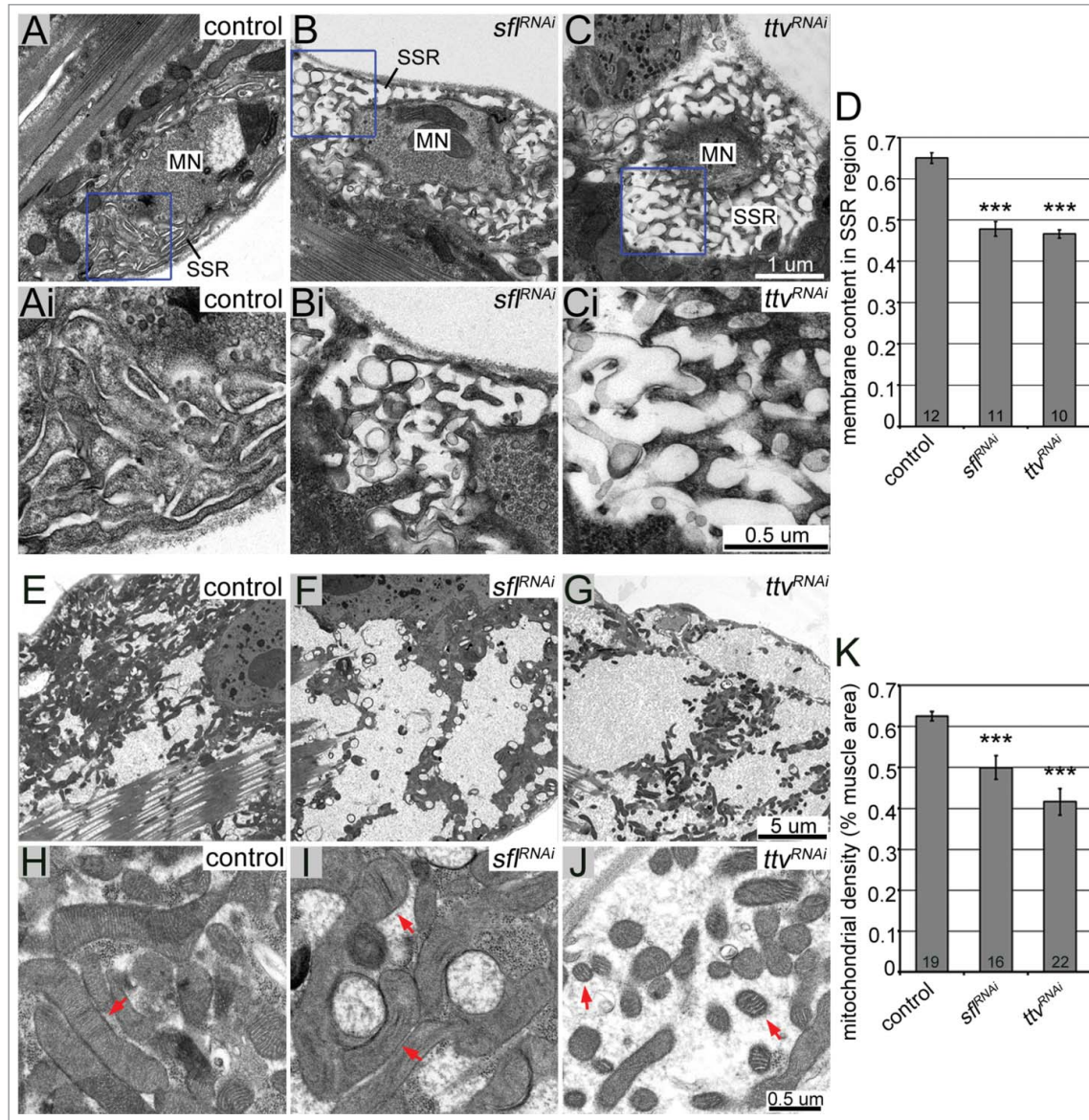


Figure 2. Changes in SSR structure, mitochondrial number and morphology in HS biosynthesis compromised larval muscles. (A to C) TEM images of the SSR at a single synaptic bouton; SSR: subsynaptic reticulum; MN: motoneuron. In control animals (A and Ai: *Mef2-GAL4*+/+), SSR comprised of multiple compactly assembled membrane stacks are tightly packed surrounding the presynaptic nerve terminal. In animals where *sfl* (B and Bi: *Mef2-GAL4*>UAS-*sfl* RNAi) or *ttv* (C and Ci: *Mef2-GAL4*>UAS-*ttv* RNAi) function was compromised by muscle-directed RNAi, SSR organization was disrupted. (Ai to Ci) Higher magnification views of regions demarked by blue squares in (A to C). (D) Quantitative analysis of membrane content in the SSR showed significant decreases in *sfl* RNAi and *ttv* RNAi-expressing muscles compared with controls. (E to G) TEM micrographs of the cytoplasm below the NMJ synapse in controls (E: *Mef2-GAL4*+/+) and animals expressing *sfl* RNAi (F: *Mef2-GAL4*>UAS-*sfl* RNAi) or *ttv* RNAi (G: *Mef2-GAL4*>UAS-*ttv* RNAi) in the muscle. Note the paucity of mitochondria in *sfl* RNAi and *ttv* RNAi compared with controls. (H and I) Electron micrographs of mitochondrial morphology in controls (H), and animals expressing *sfl* RNAi (I) or *ttv* RNAi (J) in the muscle. Red arrows indicate individual mitochondria of interest. In I, controls show mostly rod shaped mitochondria, while RNAi against *sfl* or *ttv* lead to a large number of mitochondria that were "bent" or shorter and rounder. (K) Quantification of mitochondrial density in the subsynaptic cytosol. Compared to controls, *sfl* RNAi and *ttv* RNAi-expressing animals have fewer mitochondria. Scale bars (A to C) 1 μ m, (Ai to Ci) .5 μ m, (E to G) 5 μ m, (H to J) 0.5 μ m. Error bars denote SEM. ***, $P < 0.001$. Numbers at the bottom of the bar indicate sample sizes.

change was measured by determining the membrane area (the electron dense membrane bilayer) divided by the total area encompassed by the SSR (with the motoneuron terminal area subtracted out). Membrane elaboration was significantly reduced in animals with either *sfl* or *ttv* RNA interference in the muscle cell (Fig. 2 D). Per unit area of the postsynaptic specialization, less membrane complexity is found within the SSR of animals with compromised HS biosynthesis.

TEM analysis of animals with RNAi against *sfl* or *ttv* revealed other changes in the muscle cell. Mitochondria were reduced in number (Fig. 2 E to G and K) and altered in their morphology (Fig. 2 H to J). In control animals mitochondria were elongated and cylindrical (Fig. 2 H) whereas in both *sfl* and *ttv* RNAi-bearing animals mitochondria were more elliptical (Fig. 2 I and J), in some cases horseshoe-shaped in cross-section (see *sfl* RNAi in Fig. 2 I).

Another notable feature observed in the TEM images was an abundance of double-membrane vesicular structures (Fig. 3 A, B, and D), particularly in *sfl* RNAi-bearing animals, where their density was significantly increased compared with controls (Fig. 3 C). Many of these intracellular structures had material

between the 2 membrane layers (Fig. 3 B, Bi, D, and Di show these structures in *sfl* RNAi and *ttv* RNAi-bearing animals), an organization not associated with mature autophagosomes. These double-membrane structures were often found in close proximity to mitochondria (Fig. 3 Di). The outer membrane of mitochondria has been shown to contribute to autophagosome biogenesis in mammalian cells,²⁴ suggesting the possibility that these vesicular structures are an intermediate in autophagosome formation, and that autophagy is altered in muscle cells with compromised HS production.

Autophagy is a process where cytoplasmic components are enveloped and delivered to lysosomes for degradation.²⁵ A number of proteins are critical for the formation of autophagosomes and delivery of cargo destined for degradation. *ref(2)P* is a receptor protein that binds to both ubiquitin-modified proteins and Atg8a, a ubiquitin-like protein required for autophagy and covalently attached to the outer membrane of the assembling autophagosome. The levels and cellular distribution of *ref(2)P* provide a measure of changes in autophagy, and anti-*ref(2)P* antibodies were used to examine cells with RNA interference of HS-biosynthetic components. Consistent with studies of

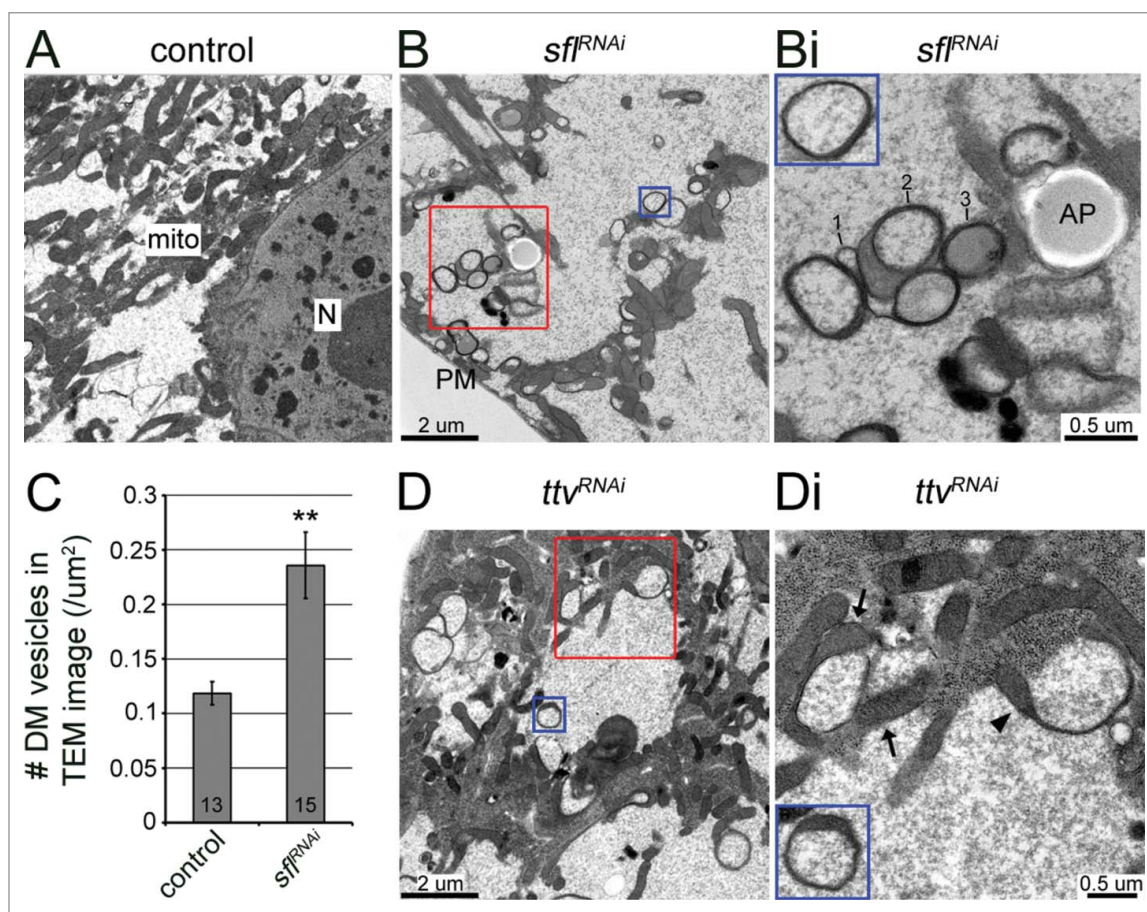


Figure 3. Accumulation of membrane-bound structures in muscle cells of larvae with compromised HS biosynthesis. (A, B and Bi) Electron micrographs of subsynaptic cytosol in controls (A: *Mef2-GAL4*^{-/-}) and animals expressing *sfl* RNAi in the muscle (B and Bi: *Mef2-GAL4*[>]UAS-*sfl* RNAi). (Bi) Higher magnification view of structures in the red box (whole panel) and the blue box (inset) from (B). In addition to classical autophagosomes, there are groups of membrane bound structures, some with single membrane layers (1), or nested within one another (2), and double-membrane-bound structures filled with electron dense material (3) and cytosol (inset). *Mef2-GAL4*[>]UAS-*sfl* RNAi animals have many more vesicular structures than controls, quantified in (C). mito: mitochondria; N: nucleus; AP: autophagosome, PM: plasma membrane. (D) *Mef2-GAL4*[>]UAS-*ttv* RNAi animals harbor similar membranous structures. (Di) A higher magnification view of the red-boxed area in (D) (whole panel) and the blue box (inset). Vesicles appear adjacent to mitochondria (arrows). Crescent shaped thick membrane sheets containing regions of mitochondrial matrix (arrowhead) and closed vesicles with mitochondrial matrix-like material remaining between the layers (inset) are common. Scale bars: 2 μm (A and B as well as D), 0.5 μm (Bi and Di). Error bars denote SEM. **, $P < 0.01$. Numbers at the bottom of the bars indicate sample sizes.

autophagy in other *Drosophila* cell types, blockade of autophagy by RNAi against *Atg8a* in larval muscle produced an elevated level of ref(2)P-positive puncta in the cytoplasm.^{26,27} This is accompanied by an increase in ubiquitin-modified proteins that

largely colocalize with the ref(2)P-positive structures (Fig. 4, compare A to H, and B to I). Overexpression of *Atg8a*^{28,29} or inhibition of the Akt-MTOR signaling pathway^{30,31} through RNAi inhibition of the *Drosophila* class I phosphatidylinositol 3-

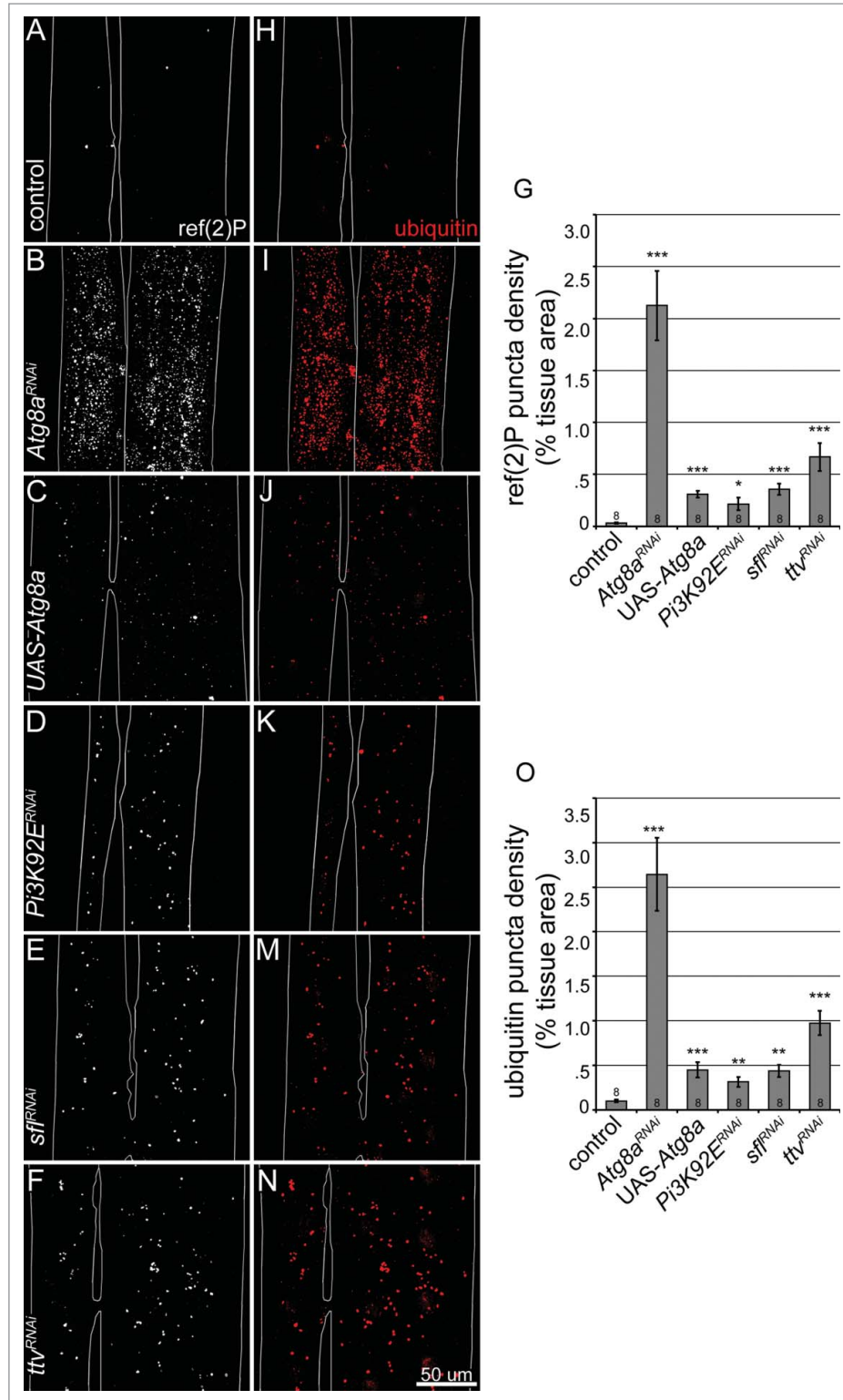


Figure 4. Compromised HS biosynthesis leads to increased levels of autophagy indicator proteins in larval muscle. (A to F) Confocal images of anti-ref(2)P and (H to N) anti-ubiquitin immunostaining of muscles 6 and 7, segment A3, in 3rd instar larvae. (A and H) control: *Mef2-GAL4>UAS-w* RNAi, (B and I) inhibition of autophagy: *Mef2-GAL4>UAS-Atg8a* RNAi, (C and J) enhanced autophagy (overexpression of *Atg8a*): *Mef2-GAL4>UAS-Atg8a*, (D and K, enhanced autophagy): *Mef2-GAL4>UAS-Pi3K92E* RNAi, (E and M): *Mef2-GAL4>UAS-sfl* RNAi, (F and N): *Mef2-GAL4>UAS-ttv* RNAi. (G) Quantification of ref(2)P immunofluorescent signal density. (O) Quantification of ubiquitin immunofluorescent signal density. Scale bar: 50 μm. Error bars denote SEM. *, *P* < 0.05; **, *P* < 0.01; ***, *P* < 0.001. Numbers at the bottom of the bars indicate sample sizes.

kinase *Pi3K92E*, conditions shown to increase autophagy in other cell types, also increased the levels of ref(2)P and ubiquitin intracellular puncta, although to a much lesser degree (Fig. 4 C and J, D and K), presumably reflecting the increase in molecules destined for destruction. RNA interference of either *sfl* or *ttv* also produced an increase in both ref(2)P and ubiquitin-modified proteins in muscle cells (Fig. 4 E and M, F and N). The increase in both markers in response to *sfl* and *ttv* RNAis was on a scale similar to that seen in *Atg8a* overexpression and *Pi3K92E* RNAi, rather than the drastic accumulation achieved with knockdown of *Atg8a* (Fig. 4 G and O). These results indicate that autophagy is disrupted in muscle cells with compromised HS biosynthesis but do not address whether there is a blockade or conversely an increase in autophagic flux.

Changes in autophagy mediated by compromising HS-biosynthesis were further examined by monitoring both early and late elements of the degradative process (Fig. 5). Ectopically expressed GFP-tagged Atg8a has been widely used to monitor the levels and cellular distribution of autophagosomes.³² A vital dye, LysoTracker Red selectively accumulates within acidic intracellular compartments, mainly lysosomes and autolysosomes

(generated by autophagosome-lysosome vesicle fusion), providing a measure of delivery of material to the degradative machinery.³² RNAi against either *sfl* or *ttv* significantly increased the numbers of GFP-Atg8a-labeled structures (Fig. 5 A to C and G) and LysoTracker Red-positive vesicles (Fig. D to F and H). These findings show that disruptions of HS-synthesis increased intracellular structures associated with autophagic degradation from early to late steps and provide evidence that changes in ref(2)P-positive or Atg8a-tagged components were not the consequence of a blockade in progression to lysosomes.

Together, the increase in both GFP-Atg8a and LysoTracker Red-positive vesicles in animals with decreased HS biosynthesis is consistent with an increased flux of material through the autophagy process. To monitor this process directly we used a form of Atg8a that is tagged with both GFP and mCherry fluorescent epitopes.³³ This construct produces both GFP and mCherry fluorescence in nonacidic compartments, but GFP emission is lost when the molecule arrives in the lysosome, where protonation destroys the structure necessary for GFP but not mCherry fluorescence.^{34,35} Thus, GFP and mCherry double-fluorescing structures (yellow) provide a measure of the

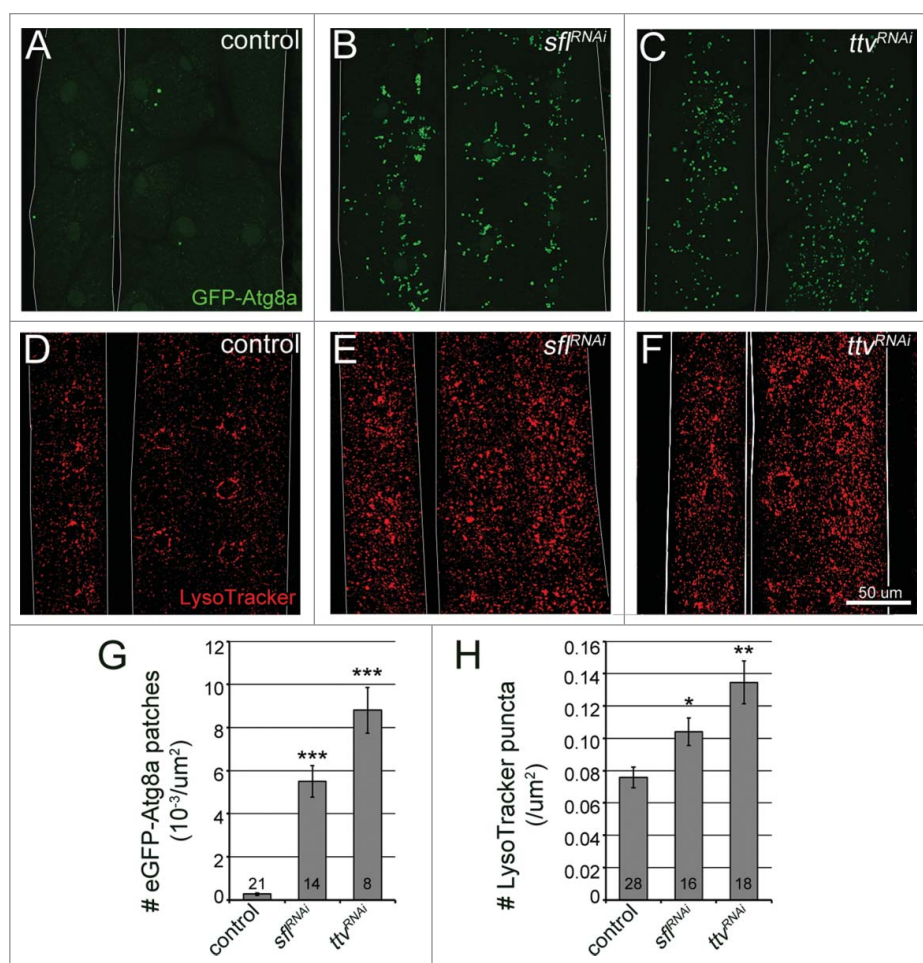


Figure 5. Accumulation of autophagic structures in muscle cells of larvae with compromised HS biosynthesis. (A to C) Confocal images of muscles 7 and 6 in controls (A: *Mef2-GAL4>UAS-GFP-Atg8a*) and animals also expressing RNAi constructs targeting *sfl* (B: *Mef2-GAL4>UAS-GFP-Atg8a; UAS-sfl* RNAi) or *ttv* (C: *Mef2-GAL4>UAS-GFP-Atg8a; UAS-ttv* RNAi). Autophagosomes were visualized with GFP-Atg8a. (D to F) Autophagy levels were measured with LysoTracker Red in controls (D: *Mef2-GAL4/+*) and animals with muscle-specific expression of *sfl* RNAi (E: *Mef2-GAL4>UAS-sfl* RNAi) or *ttv* RNAi (F: *Mef2-GAL4>UAS-ttv* RNAi). (G) Average number of GFP-Atg8a-positive patches. (H) Average number of LysoTracker Red-positive structures. Scale bar: 50 μm . Error bars denote SEM. *, $P < 0.05$; **, $P < 0.01$; ***, $P < 0.001$. Numbers at the bottom of the bars indicate sample sizes.

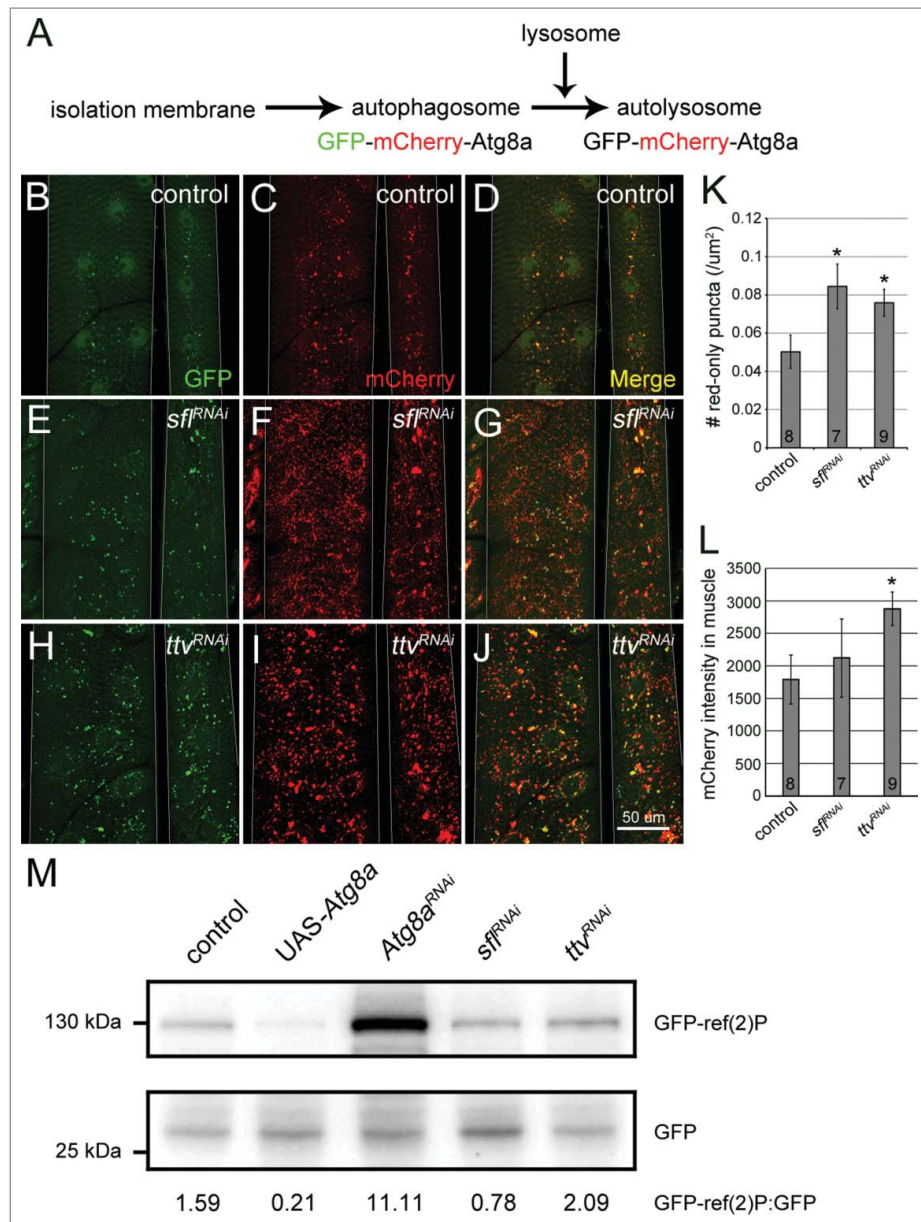


Figure 6. Reductions in HS biosynthesis and modification, result in a net increase in autophagic flux. (A) Changes in autophagic flux were monitored using a GFP-mCherry-Atg8a marker in muscles 6 and 7 of third instar larvae. (B to J) Early autophagosomes show both GFP and mCherry fluorescence. Autolysosomes are labeled solely with mCherry fluorescence as the acidic environment quenches GFP signal. Controls (B to D: *Mef2-GAL4>UAS-GFP-mcherry-Atg8a*), larvae with muscle-directed RNAi against *sfI* (E to G: *Mef2-GAL4>UAS-GFP-mcherry-Atg8a; UAS-sfI RNAi*) or *ttv* (H to J: *Mef2-GAL4>UAS-GFP-mcherry-Atg8a; UAS-ttv RNAi*). Merged images showed several mCherry-labeled patches were not colabeled with GFP in (G) *sfI* RNAi and (J) *ttv* RNAi-expressing muscle cells. (K) Compared with controls, muscles expressing RNAi constructs of *sfI* or *ttv* showed significantly more mCherry-exclusive puncta. (L) Fluorescent intensity of mCherry was similar to that of controls in *sfI* RNAi and significantly increased in *ttv* RNAi-expressing animals. (M) An anti-GFP western blot to examine lysosomal degradation of exogenous GFP-ref(2)P expressed ubiquitously under the control of *da-GAL4* in total protein extracts of whole third instar larvae. The intact fusion protein migrates at approximately 130 kDa (upper box) while the free GFP domain released by lysosomal degradation runs at approximately 27 kDa (lower box). The ratio of fusion protein to free GFP, calculated by division of background-corrected GFP-ref(2)P band signal density by free GFP background-corrected intensity within each sample, is displayed below the bottom box. *da-GAL4>UAS-GFP-ref(2)P* without an additional transgene served as the control. Scale bar: 50 μm (B to J). Error bars denote SEM. *, $P < 0.05$. Numbers at the bottom of the bars indicate sample sizes.

number of early autophagosomes, whereas structures with only mCherry signal (red) indicate the relative number of autolysosomes (Fig. 6 A). In control animals, a proportion of the mCherry fluorescence overlapped with the GFP fluorescence, consistent with the shared labeling of early autophagosomes (Fig. 6 B to D). In animals bearing either *sfI* or *ttv* RNAi constructs, the levels of GFP and mCherry double-positive vesicles were elevated compared with control animals (Fig. 6 E to J). In addition, the number of mCherry-exclusive fluorescing

structures was significantly increased in both *sfI* and *ttv* RNAi-bearing animals compared with controls, with mCherry fluorescent intensity also significantly increased by *ttv* inhibition (Fig. 6 K and L). These findings are consistent with published reports documenting the behavior of this molecular reporter under conditions of a net increase in autophagic flux.³²

We also investigated the previously identified increase in endogenous ref(2)P levels pursuant to its implication in autophagic flux. Pancellular ectopic expression of a GFP-ref(2)P

fusion protein was used to examine the efficacy of ref(2)P degradation in HS biosynthetically impaired animals by comparing levels of free GFP to levels of the parental GFP-ref(2)P protein.^{32,36–38} An anti-GFP western blot revealed that proteolytic release of free GFP (~27 kDa) from GFP-ref(2)P (~130 kDa), as measured by the ratio between these 2 protein species, was increased in animals overexpressing *Atg8a* to enhance autophagic degradation. Treatment with RNAi against *Atg8a* to inhibit autophagy resulted in a pronounced accumulation of the GFP-ref(2)P fusion protein (Fig. 6 M). Conversion of GFP-ref(2)P to free GFP was increased in *sfl* RNAi similar to the effect seen in *Atg8a* overexpression, indicating that while endogenous ref(2)P levels may be increased in these animals, this does not reflect reduced degradative capacity. Inhibition of *ttv* caused a modest increase in the ratio of fusion protein to free GFP, however, this effect was mild in comparison to inhibition of *Atg8a*. In combination with the analysis of the GFP-mCherry-*Atg8a*, these results suggest that autophagosome maturation proceeds normally, and the increase in autophagy components indicates an overall increase in autophagic degradation.

A number of experiments were conducted to determine if the effect of HS biosynthesis on autophagy in muscle was a direct or indirect effect. Disrupting HS synthesis in muscle could potentially affect feeding behavior or otherwise produce systemic activation of autophagy. Systemic autophagy can be monitored by examining levels of autophagy markers in the fat body, the principal energy storage and nutritional sensing organ in *Drosophila*. Muscle-specific RNAi of *sfl* and *ttv* did not induce an increase in LysoTracker Red staining in the fat body, a response readily observed with starvation (Fig. S2 A to C, as well as H, L and M). We also monitored food ingestion in animals with RNAi of HS biosynthesis in muscle using fluorescein, a fluorescent dye incorporated in the food.³⁹ Animals expressing muscle-directed RNAi of *sfl* had comparable levels of food ingestion compared with wild-type larvae (data not shown). We also determined that a starvation protocol that produces robust activation of autophagy in the fat body (Fig. S2 D, H, and M), produced no change in either LysoTracker Red or *Atg8a*-GFP markers in the muscle (Fig. S2 D to G, H to K, and M to O). Collectively these experiments show that RNAi of genes required for HS biosynthesis in the muscle produced elevated levels of autophagy independent of nutritional or systemic activation of autophagy, and that body wall muscles do

not show a nutritional stress response as sensitive to starvation as that documented for the fat body.

We also evaluated whether disruption of HS-biosynthesis could alter the secretory apparatus in some manner and activate ER stress, a known trigger of autophagy.^{40,41} Activation of ER stress mediated by Ire1^{42–44} produces alternative splicing of an *Xbp1* transcript engineered to create an open reading frame for eGFP translation only after splicing. This construct has been used successfully as a sensitive indicator of ER stress activation.⁴⁵ RNAi of *sfl* or *ttv* in the muscle, conditions that produce elevated autophagy, did not result in activation of the ER-stress reporter, while expression of a misfolded version of the *ninaE* protein (*ninaE*^{G69D})^{45,46} produced a robust response (Fig. S3). By this measure, elevated autophagy in animals with RNAi of HS biosynthesis was not produced by activation of an ER stress response.

Autophagosome and mitochondrial association in *sfl* RNAi animals

Selective autophagic elimination of mitochondria, referred to as mitophagy, provides a mechanism to regulate mitochondrial numbers and remove damaged organelles.^{47,48} In *sfl* and *ttv* RNAi-expressing muscle, autophagosomes were found in the vicinity of mitochondria (Fig. 3 Di). The reductions in mitochondrial densities were also accompanied by changes in their morphology. Instead of the typical rod-like, elongated mitochondria seen in control animals, *sfl* RNAi produced curved or cup-like mitochondria (Fig. 2 H and I). Reduction of *ttv* function resulted in more rounded mitochondria (Fig. 2 J). The proximity of vesicular structures that bear molecular tags of autophagosomes near mitochondria was of interest for 2 reasons. First, it would inform the possibility that autophagosomal elements could derive at least in part from mitochondria, a phenomenon documented in mammalian cells.²⁴ Second, the loss of mitochondria in the muscle cells of animals with defective HS biosynthesis could result from either a “conversion” of mitochondria to autophagosomal structures or mitophagy directly. Mitochondria and autophagosomes were examined simultaneously using a monoclonal mitochondria-specific antibody 4C7 and GFP-*Atg8a*. Visualization of mitochondria (red) and autophagosomes (green) showed some mitochondria in *sfl* RNAi muscles in close association with autophagosomes (Fig. 7 A to C), and mitochondria enveloped by GFP-*Atg8a*-positive

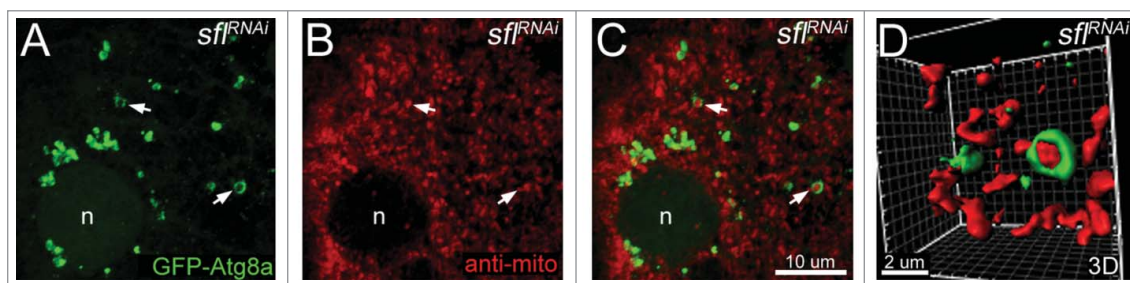


Figure 7. Proximity of mitochondria and autophagosomes in *sfl* RNAi-expressing animals. (A to D) Autophagosomes were visualized with GFP-*Atg8a* (green) and mitochondria were detected with anti-mitochondria antibody (red) in *sfl* RNAi expressing muscle (*Mef2-GAL4>UAS-GFP-Atg8a; UAS-sfl* RNAi). Autophagosomal vesicles containing mitochondrial spheroids are indicated by arrows. (D) Three-dimensional reconstruction from serial confocal optic sections depicting autophagosomal and mitochondrial localizations in an animal expressing the *sfl* RNAi construct. Some optical sections not included to reveal interior of structure. n, nuclei. Scale bars: 10 µm (A to C), 2 µm (D).

structures (Fig. 7 C and D; the high magnification view shown in D provides a cross-section of a mitochondrion surrounded by a GFP-Atg8a-tagged autophagosome, the 3D-reconstruction includes several confocal optical sections, but not the entire set which showed envelopment of the mitochondrion). These findings suggest a role of autophagy in the reduction of mitochondrial number in animals with compromised HS biosynthesis (Fig. 2 K).

HS biosynthesis is required for suppression of autophagy in fat body and is noncell autonomous

Given the profound effects of abrogating HS-polymer biosynthesis or sulfation on autophagy in developing muscle, it was of interest to determine if this regulatory relationship exists in other cell types. The requirement for HS biosynthesis in muscle for the normal regulation of autophagy suggested the possibility that HSPGs serve this function in multiple tissues. To assess this hypothesis, the level of autophagy in fat body cells was evaluated in animals with compromised HS biosynthesis. The fat body is a tissue central to energy storage and utilization, and mounts a robust autophagic response during periods of nutritional stress, characterized by increased levels of both autophagosomes and lysosomes.⁴⁹ RNA interference of *sfl* or *ttv* directed to the fat body with *r4-GAL4* produced significant increases in GFP-Atg8a labeled intracellular structures (Fig. 8 A to D) as well as LysoTracker Red-positive organelles (Fig. 8 E to H) indicating that loss of HS biosynthesis permits activation of autophagy in the absence of starvation in this tissue. The importance of HS biosynthesis in regulation of autophagy in the fat body was further examined using a *ttv* mutant that survives to the third instar larval stage. Larvae homozygous for *ttv*⁰⁰⁶⁸¹ showed dramatic increases in LysoTracker Red-positive structures in the fed state (Fig. 9 A to C), consistent with the RNAi experiments.

The robust activation of autophagy in fat body of *ttv* mutant larvae provided the tool for addressing an important mechanistic question: Is HS biosynthesis required cell autonomously, or can neighboring cells with normal HS production provide the function to achieve normal autophagy regulation? A non-cell autonomous function would support a mechanism that requires signaling in the extracellular space, where HSPGs are known to regulate the activity of several growth factor pathways that influence regulators of autophagy, most notably PI3 kinase. Using a system for inducing mitotic recombination in the fat body to produce *ttv*^{00681/ttv}⁰⁰⁶⁸¹ (Fig. 9 D, cells without expression of a GFP marker) and *+/+* cell clones (Fig. 9, bright green cells, bearing 2 copies of GFP-expressing marker gene construct) from *ttv*^{00681/+} heterozygous parental cells, genetic mosaics were created in third instar larval fat body. LysoTracker Red-positive structures were not elevated in *ttv*^{00681/ttv}⁰⁰⁶⁸¹ cell clones (Fig. 9 E). In all 15 cases examined, the mutant cells were in contact with either *ttv*^{00681/+} or *+/+* cells, a common occurrence in fat body, where large isolated mutant clones are rare. These experiments demonstrated that *ttv* function was not required in a cell to maintain normal levels of autophagy under conditions where it was in

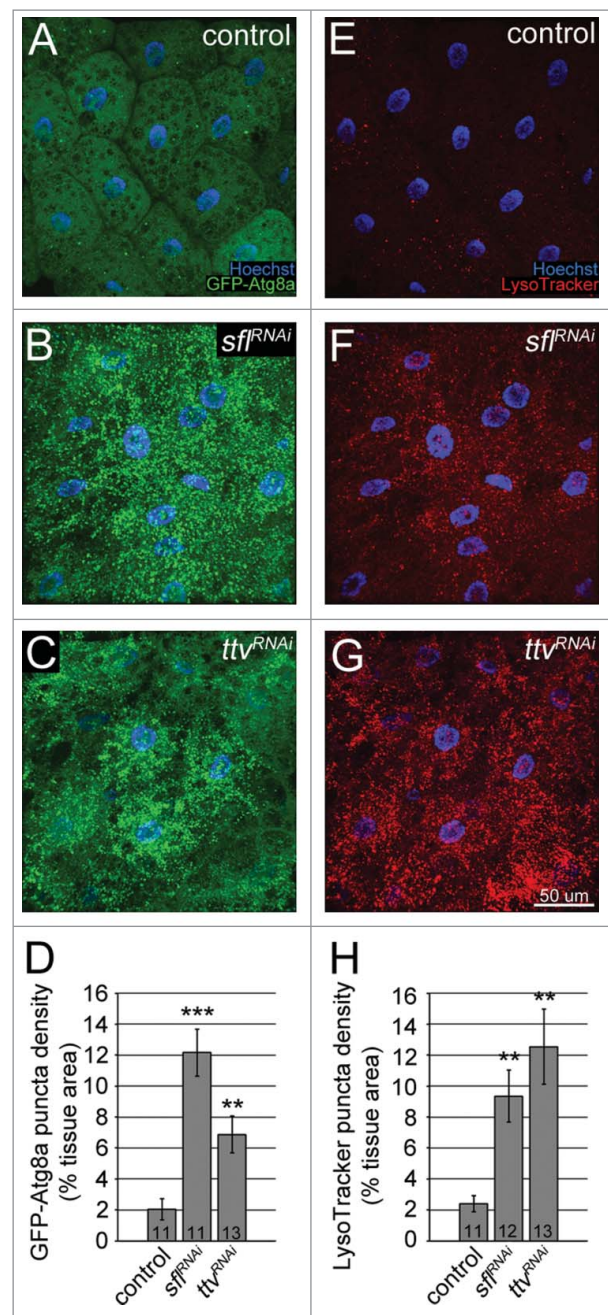


Figure 8. Inhibition of HS biosynthesis in fat body cells induces autophagy in fed larvae. (A to C) Confocal images showing increased numbers of GFP-Atg8a-positive autophagosomes in fat body cells of animals expressing RNAi constructs targeting *sfl* (B, F: *r4-GAL4*>UAS-GFP-Atg8a; UAS-*sfl* RNAi) or *ttv* (C, G: *r4-GAL4*>UAS-GFP-Atg8a; UAS-*ttv* RNAi) compared with controls (A, E: *r4-GAL4*>UAS-GFP-Atg8a; UAS-*w* RNAi). Autophagosomes were visualized by GFP-Atg8a (green), and nuclei were stained with Hoechst (blue). (D) The average density of GFP-Atg8a puncta was significantly increased in animals expressing *sfl* RNAi or *ttv* RNAi in comparison to animals expressing *w* RNAi (control) or no RNAi construct (not shown). (E to G) Within the same animals, autophagic degradation was measured by staining with LysoTracker Red to visualize acidic organelles. (F) The average density of LysoTracker Red puncta was significantly increased in animals expressing *sfl* RNAi or *ttv* RNAi in comparison to animals expressing *w* RNAi (control) or no RNAi construct (not shown). Scale bar: 50 μ m. Error bars denote SEM. *, $P < 0.05$; **, $P < 0.01$; ***, $P < 0.001$. Numbers at the bottom of the bars indicate sample sizes.

contact with other HS-producing cells. This result shows that some signaling process in the extracellular space is required for the normal suppression of autophagy by HSPGs.

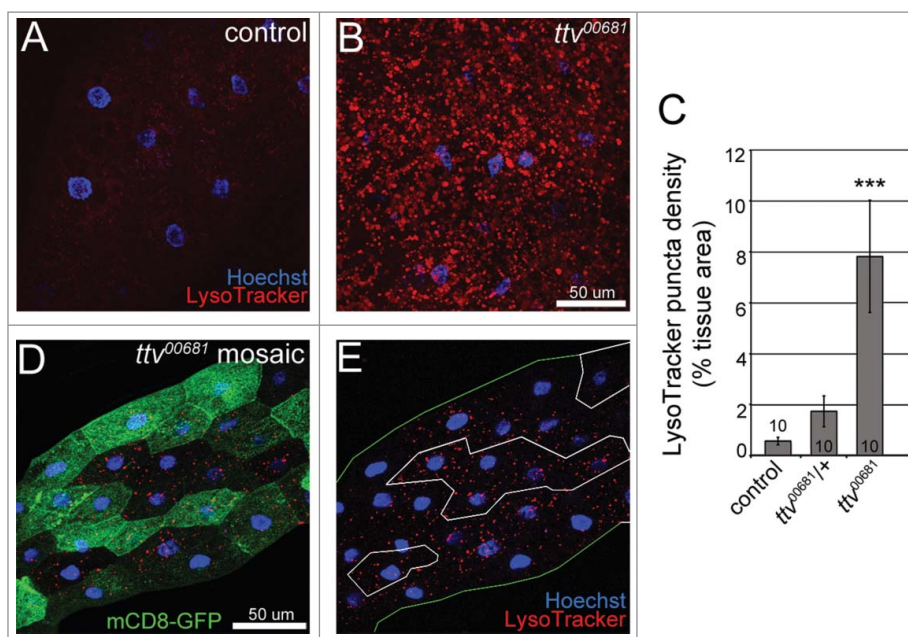


Figure 9. Homozygous mutant *ttv*⁰⁰⁶⁸¹ causes a cell non-autonomous increase in the number of acidic organelles. (A and B) Confocal images of unfixed fat body tissue from wandering 3rd instar larvae. Acidic organelles visualized using LysoTracker Red and nuclei visualized using Hoechst (blue) in control (A: Oregon R) and homozygous mutant (B: *ttv*⁰⁰⁶⁸¹) larvae. (C) Density of LysoTracker Red-positive puncta was significantly increased in homozygous mutants. (D and E) Homozygous *ttv*⁰⁰⁶⁸¹ clones were generated by heat shock-induced FRT mediated recombination in a heterozygous background. (D) The wild-type chromosome arm is marked with UAS-mCD8 GFP, which appears the brightest in homozygous wild-type cells, while homozygous mutant cells are identified by the absence of GFP. (E) Green lines indicate tissue boundaries. White lines demark homozygous *ttv*⁰⁰⁶⁸¹ mutant clones. The density of acidic organelles marked by LysoTracker Red is similar in homozygous mutant clones and neighboring heterozygous cells or wild-type clone cells. Scale bars: 50 μm. Error bars denote SEM. ***, $P < 0.001$. Numbers at the bottom of the bars indicate sample sizes.

Compromising *Atg* gene function rescues SSR and mitochondrial phenotypes in animals with reduced *sfl* function

The findings described above establish that HS biosynthesis is an important determinant of autophagy levels in 2 cell types, muscle and fat body. Compromising HS assembly and hence HSPG structure also has morphological and functional consequences in muscle tissue. To determine if the change in autophagy mediated by altered HS biosynthesis was responsible for these phenotypes, we investigated whether inhibiting expression of known autophagy genes could ameliorate phenotypes associated with compromised HS assembly. TEM analysis revealed that changes in SSR morphology and membrane content of the postsynaptic muscle cell that accompanied interference of *sfl* were suppressed with expression of an RNAi construct directed against *Atg8a* (Fig. 10 A to D). This reduction in *Atg8a* function also served to rescue the changes in mitochondrial density found in *sfl* RNAi muscle cells (Fig. 10 E).

The interplay between HS-biosynthesis and autophagy levels in affecting muscle phenotypes was further explored using RNAi constructs directed against other autophagy components. Scoring animals for mitochondrial morphology, RNAi against *Atg5*, *Atg7*, or *Atg8a* reduced the degree of mitochondrial morphological abnormality compared with animals expressing *sfl* RNAi alone (Fig. 10 F). These findings support the conclusion that HS-mediated regulation of autophagy is an important function of these molecules, affecting both the assembly of an important postsynaptic membrane specialization and the density of mitochondria at this energy-demanding cell-cell contact.

Reducing the levels of autophagy in animals with compromised HS biosynthesis rescues lethality

HS biosynthesis is required for viability; animals bearing mutations in key enzyme-encoding genes show developmental arrest and do not survive to the adult stage.¹¹ The stage of arrest is affected by the point during development at which gene function is compromised, and the degree of functional loss induced by any particular allele.^{11,50-53} Consistent with published work describing mutant alleles, RNAi against *sfl* and *ttv* using a ubiquitously-expressed *GAL4* transcriptional activator, *Da-GAL4*, produced lethality at second instar larval and early-pupal stages, respectively (Table 1). To determine if the lethality produced by reduction of *sfl* or *ttv* function is due in some measure to elevated levels of autophagy, we examined the development of animals with both compromised HS biosynthesis and reduced *Atg* gene function. Ubiquitous expression of RNAi constructs directed against *Atg8a*, *Atg5*, and *Atg7* all partially rescued lethality in *sfl* RNAi and *ttv* RNAi-expressing animals, improving the survival stage from the second instar larval stage to mid-pupal stage and early-pupal to mid-pupal stage, respectively (Table 1). QPCR of animals expressing these constructs was done to assess the levels of *sfl*, *ttv*, and *Atg* gene mRNAs (Fig. S1 G). These experiments showed that *sfl* and *ttv* mRNA levels were not affected by *Atg* RNAi constructs and vice versa, indicating the interaction was at the level of autophagy function. Expression of *UAS-GFP* did not produce any improvement in survival, showing that the rescue was due to the reduced activities of the *Atg* genes, and not the presence of an additional *UAS* transgene (Table 1).

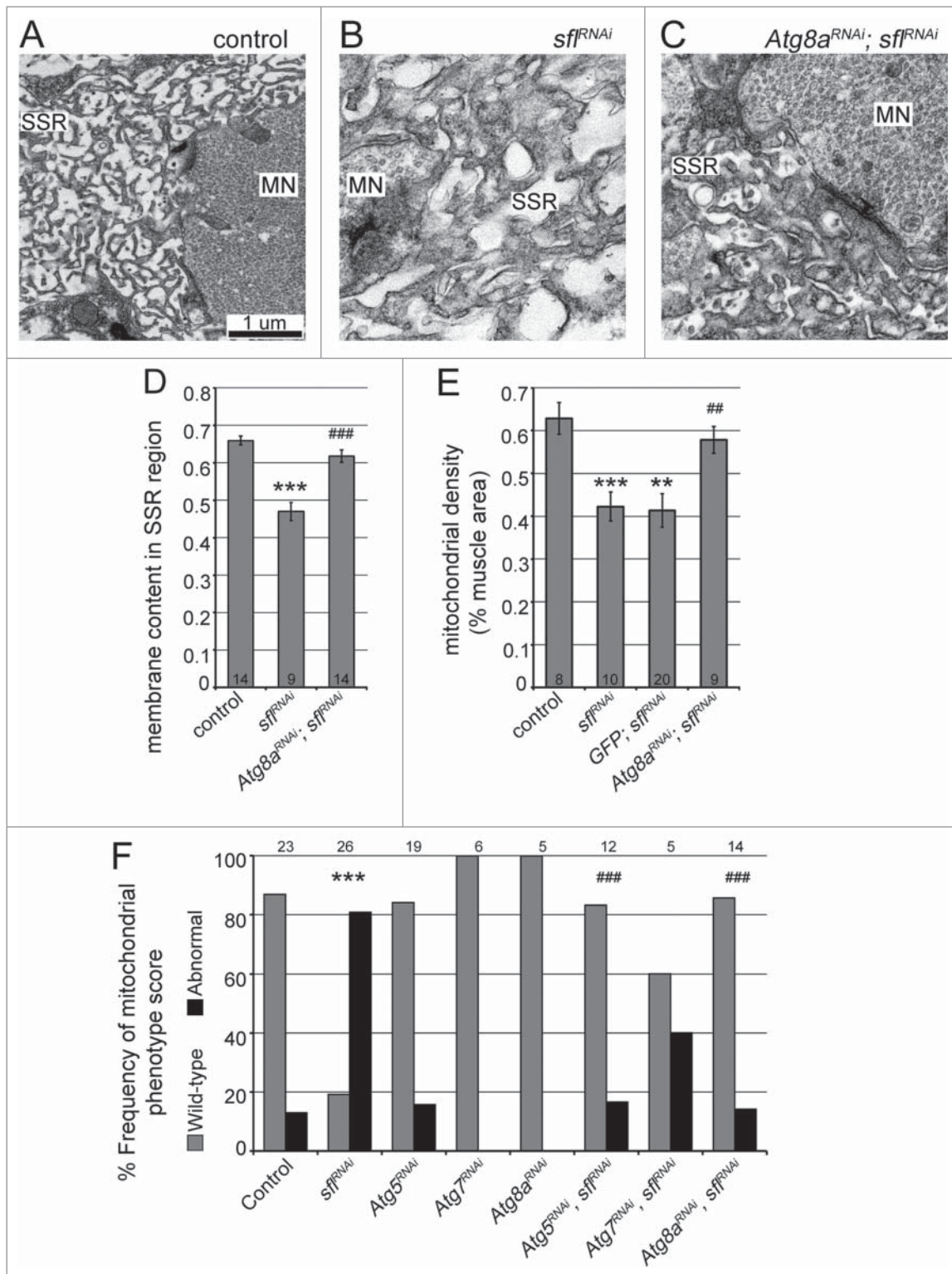


Figure 10. Mitochondrial and SSR phenotypes associated with impaired HS modification are suppressed by downregulation of autophagy. (A to C) Ultrastructure of SSR in control (A: *Mef2-GAL4*/+), *sfl* RNAi (B: *Mef2-GAL4*>UAS-*sfl* RNAi), and animals coexpressing *sfl* RNAi and *Atg8a* RNAi (C: *Mef2-GAL4*>UAS-*Atg8a* RNAi, UAS-*sfl* RNAi). Abnormally assembled SSR found in animals with loss of *sfl* function was partially rescued by expressing *Atg8a* RNAi. (D) Quantification of membrane content in the SSR region. Reduction of *Atg8a* function by expressing *Atg8a* RNAi in the muscle restored SSR membrane density in *sfl* RNAi animals to a significant degree. SSR, subsynaptic reticulum; MN, motoneuron. (E) Quantitative analysis of mitochondrial densities in TEM micrographs. Coexpression of *Atg8a* RNAi significantly increased mitochondrial density in *sfl* RNAi expressing animals. (F) Mito-GFP was used as a marker of mitochondrial morphology for confocal imaging in larval muscle. Mitochondrial phenotypes were assessed in animals expressing a control RNAi (UAS-*w* RNAi), RNAi targeting *sfl*, *Atg5*, *Atg7*, and *Atg8a* alone, and concomitant RNAi inhibition of *sfl* together with each of the *Atg* genes driven by *Mef2-GAL4*. Mitochondrial morphology in genotype blinded confocal images was scored as either 'wild type' or 'abnormal' using images from Oregon R larvae as baseline. Inhibition of *sfl* significantly increased the incidence of abnormal mitochondrial phenotypes, while the *Atg* genes and the RNAi control were not associated with a change in relative score frequencies. Coinhibition of *Atg5* or *Atg8a* with *sfl* RNAi significantly rescued the score frequencies associated with *sfl* inhibition. Coinhibition of *sfl* and *Atg7* produced an intermediate phenotype. Scale bar: 1 μ m (A to C). Error bars denote SEM. **, $P < 0.01$; ***, $P < 0.001$ for comparisons with controls. ##, $P < 0.01$; ###, $P < 0.001$ for comparisons with *Mef2-GAL4*>UAS-*sfl* RNAi. Numbers at the bottoms of the bars (D) and (E) and above the bars (F) indicate sample sizes.

Table 1. The survival stages of *Drosophila* with HS biosynthetic inhibition and inhibition of *Atg* genes.

Genotype	Viability
<i>da-GAL4/+</i>	adults
<i>da-GAL4 > UAS-sfl^{RNAi}</i>	2nd instar larvae
<i>da-GAL4 > UAS-GFP; UAS-sfl^{RNAi}</i>	2nd instar larvae
<i>da-GAL4 > UAS-Atg5^{RNAi}; UAS-sfl^{RNAi}</i>	pupae
<i>da-GAL4 > UAS-Atg7^{RNAi}; UAS-sfl^{RNAi}</i>	pupae
<i>da-GAL4 > UAS-Atg8a^{RNAi}; UAS-sfl^{RNAi}</i>	pupae
<i>da-GAL4 > UAS-ttv^{RNAi}</i>	early pupae (white pupae)
<i>da-GAL4 > UAS-GFP; UAS-ttv^{RNAi}</i>	early pupae (white pupae)
<i>da-GAL4 > UAS-Atg5^{RNAi}; UAS-ttv^{RNAi}</i>	pupae
<i>da-GAL4 > UAS-Atg7^{RNAi}; UAS-ttv^{RNAi}</i>	pupae
<i>da-GAL4 > UAS-Atg8a^{RNAi}; UAS-ttv^{RNAi}</i>	pupae

da-GAL4 was used to ubiquitously express either no construct (the control, animals experience a normal life span) or an RNAi construct targeting either *sfl* or *ttv*, alone or in combination with an RNAi construct targeting *Atg5*, *Atg7*, or *Atg8a*, or with UAS-GFP which is not predicted to effect the lethality of HS biosynthetic inhibition. Genotypes are displayed on the left and the stage to which progeny survive under standard culture conditions is displayed on the right.

Discussion

HS biosynthesis deficits produce elevated levels of autophagy in muscle and fat body

Loss of heparan sulfate biosynthesis at the NMJ produces several diverse phenotypes, affecting both motoneurons and postsynaptic muscle cells. The work described here was undertaken to understand the molecular basis of 2 remarkable postsynaptic cellular phenotypes; disruption of the SSR, a postsynaptic membrane specialization, and loss of mitochondria at the synapse. The interfering RNA-generating transgenes described here provided cell-type specific blockade of function and allowed the characterization of phenotypes that were incompletely penetrant and of lesser severity in animals bearing zygotic mutations.

Expression of interfering RNAs against 2 distinct components of the HS synthesis and modification apparatus altered the organization of the SSR, an elaborate membrane specialization that expands during development to support the synaptic function of the growing larval muscle. In animals with compromised HS biosynthesis, the SSR showed a reduction of membrane complexity indicating a deficit in either elaboration or an excess of membrane retrieval from this organelle. TEM analysis of the NMJ in these RNAi-treated animals revealed an abundance of double-membrane intracellular organelles, many of them in close proximity to mitochondria. A variety of molecular markers, including ref(2)P, Atg8a, and LysoTracker Red, were all elevated in animals with compromised HS biosynthesis. A doubly-tagged GFP-mCherry-Atg8a transgene that permits tracking of both autophagosomes and autolysosomes demonstrated that these vesicle types were increased upon compromising HS-biosynthesis, showing that loss of HS biosynthetic capacity produced a net increase in autophagy and not simply an accumulation of one vesicular intermediate.

A western blot examining release of free GFP from GFP-ref(2)P, a commonly used method for examining autophagic flux in yeast and *Drosophila*,^{26,38} provided further support for an increase in the level of autophagic degradation in HS-biosynthetically compromised animals. The increase in free GFP that accompanies ubiquitous inhibition of *sfl* gene function

indicates an increase in autophagic degradation in these animals. While the effect in *ttv*-inhibited animals is more equivocal, it is possible that both release and degradation of GFP are increased, preventing the accumulation of free GFP in these animals.

Significantly, accumulation of endogenous ref(2)P and ubiquitin in larval muscle occurs under conditions in which autophagic flux is clearly elevated, supported both by previous characterization of the *Atg8a* overexpression construct and the results of both the mCherry-GFP-Atg8a analysis and the GFP conversion assay. Interpretation of ref(2)P levels in flies has primarily been performed in conjunction with treatments spanning days or weeks, and is generally examined in the tissue of adult animals.^{27,32,54} In this context, an increase in ref(2)P indicates failure of autophagic flux. However, in the context of larval tissues, increased levels of ref(2)P have been found in fat body tissue in response to starvation²⁹ and inhibition of *Tscl*,²⁶ both positive regulators of autophagy. In the tissues of these young animals, it may be that the transcriptional upregulation of ref(2)P, which is activated in response to various positive regulators of autophagy including starvation,⁵⁵ may outweigh the increased degradation of the protein through autophagy to a greater extent than in other experimental settings.

The association of double-membrane organelles with mitochondria observed in TEM images and the close proximity between GFP-Atg8a-positive structures and anti-mito-stained structures is intriguing for 2 reasons. First, in mammalian cells it has been demonstrated that the outer membrane of mitochondria can participate in autophagosome biogenesis.²⁴ Second, it raises the possibility that the reduced number of postsynaptic mitochondria in muscle that is observed with inhibition of HS biosynthesis is a consequence of either mitophagy or some “conversion” of mitochondria to autophagosome precursors, and eventually autophagosomes and autolysosomes.

RNA interference of 2 HS biosynthetic genes in the fat body also produced elevated levels of autophagy markers, indicating that the role of HSPGs in regulating autophagy is not limited to muscle. Genetic mosaic analysis showed the requirement of HS production for the control of autophagy to be non-cell autonomous. Cells that are wild type for HS synthesis could rescue the level of autophagy in adjacent HS-deficient cells. This phenomenon has been observed for HS-dependent signaling, and supports a mechanism that involves function of HSPGs in the extracellular environment.⁵⁶

The involvement of HS biosynthesis in controlling autophagy levels in *Drosophila* begs the question as to the generality of this regulation. In human epithelial cells, degradation of HSPGs by heparinase III increased the levels of autophagic markers, consistent with our findings in *Drosophila* muscle and fat body.⁵⁷ There is also recent evidence that heparanase, an endogenous HS-cleaving enzyme, enhances autophagy. Furthermore, the proautophagic function of heparanase promotes tumor growth and chemoresistance.⁵⁸

Additional clues that HSPGs can broadly suppress autophagy come from studies of SUMF1 (sulfatase modifying factor 1). SUMF1 catalyzes a post-translational modification that is required for the activity of sulfatases, including those that degrade HS.^{59,60} Loss of SUMF1 activity is therefore predicted

to increase HS levels and hence HSPG-dependent signaling. Consistent with this model, *Sumf1* mutant mice show hyperactivation of FGF18 signaling, a known HS-dependent signaling process. Interestingly, autophagy is suppressed in *Sumf1* mutants, a finding consistent with a role for HSPGs in limiting autophagy.^{61–64} In humans, loss of *SUMF1* is responsible for multiple sulfatase deficiency (MSD),⁶⁵ a syndrome characterized by neurological deficits and bone patterning abnormalities. These findings suggest a role for HSPGs in the hypersuppression of autophagy in *Sumf1* mutant animals and MSD patients.

Mechanism of HS-dependent inhibition of autophagy

HSPGs are ubiquitous cell surface-associated proteins that influence a large number of growth factor signaling systems, many of which affect class I phosphoinositide 3-kinase (PI3K),^{6,66,67} a key activator of TOR (MTOR in mammals). TOR activity in turn serves to limit autophagy. Downregulation of PI3K activity is necessary for induction of autophagy in response to nutrient deprivation or developmentally regulated autophagy during metamorphosis.^{49,68,69} The simplest hypothesis for how HSPGs serve to suppress autophagy is that their loss compromises several signaling pathways that activate PI3K and thus reduces the inhibitory input to autophagy provided by TOR. We have made several observations that support this model (data not shown): 1) overexpression of Pi3K92E in the muscle reduced autophagy and suppressed the elevated autophagy resulting from loss of HS biogenesis, 2) reduction of Pi3K92E activity produced a mitochondrial morphological phenotype like that found in HS-compromised larvae, and 3) the mitochondrial deficit associated with loss of HS function could be rescued by increasing Pi3K92E activity. These findings are suggestive, but not a direct demonstration, that HS biosynthesis affects autophagy levels via regulation of class I PI3K activity. This mechanism is best evaluated in a system where HS-directed events are elevated and their dependence on PI3K activity can be directly tested.

Autophagic regulation of postsynaptic specializations

Compromising HS biosynthesis produced loss of mitochondria in the postsynaptic cell and disruption of the SSR, a postsynaptic specialization that expands during synaptic growth and is responsive to synaptic activity.²¹ The SSR and mitochondrial phenotypes in the muscle cell were rescued by reducing the function of genes critical for autophagy, demonstrating that these cellular changes were a consequence of increased autophagy. These results provide evidence that the precise control of autophagy is critical for the assembly of postsynaptic membrane specializations; enhancing autophagy decreased the complexity of the SSR membrane structure. These findings are in concert with recent work describing the role of autophagy in dendritic spine elaboration and pruning.⁷⁰ Hyperactive MTOR produced both reductions in autophagy and a deficiency in dendritic pruning in mouse cortical projection neurons. This Tor-mediated increase in dendritic spine density could be rescued by inhibition of Tor by rapamycin, and the rescue required autophagy gene function. Our data support this link between autophagy and the control of postsynaptic specializations.

Autophagy has been previously implicated in synaptic growth in *Drosophila*, negatively regulating the level of the E3 ubiquitin ligase hiw (highwire) in the motoneuron.⁷¹ However, its function in postsynaptic development has not been as well studied. In *C. elegans*, loss of presynaptic inputs at the NMJ results in postsynaptic GABA_A receptor trafficking to autophagosomes, a mechanism for selective removal of this neurotransmitter receptor.⁷² Autophagy could affect postsynaptic function in several ways, controlling degradation of key receptors or cytoskeletal elements, altering membrane trafficking, and affecting the number of mitochondria localized at synapses to provide for the high-energy demands of synaptic transmission. In short, the precise regulation of autophagy in the nervous system is critical: modest decreases achieved by activation of Tor can result in a failure of dendritic pruning leading to behavioral deficits,²¹ and complete abrogation of autophagy produces neuronal death. The work reported here demonstrated that elevated autophagy also has consequences, decreasing the membrane complexity of postsynaptic specializations and reducing mitochondrial density at synapses.

Materials and methods

Fly husbandry

Fly strains were raised on standard cornmeal/sucrose/agar media at 25°C during embryogenesis and 30°C during larval development under a 12 h day/12 h night unless otherwise specified. Oregon-R, w¹¹¹⁸, and VDRC60100 strains served as wild-type stocks. RNAi strains and a control strain with the same genetic background were obtained from the Vienna *Drosophila* RNAi Center (VDRC)⁷³: UAS-*Atg8a* RNAi (43097), UAS-*Pi3K92E* RNAi(38985), UAS-*sfl* RNAi(5070), UAS-*ttv* RNAi(4871), UAS-*w* RNAi (30033) and empty vector control (60100). UAS-*GFP-mcherry-Atg8a*, UAS-*mCD8-GFP*, UAS-*GFP*, UAS-*mito-GFP*, EP-*Atg8a*, and the *Drosophila* Transgenic RNAi Project (TRiP)⁷⁴ lines UAS-*Atg5* RNAi (JF02703) and UAS-*Atg7* RNAi (JF02787) were obtained from the Bloomington *Drosophila* Stock Center (BDSC). UAS-*GFP-Atg8a*⁷⁵ and UAS-*GFP-ref(2)P*⁷⁶ are generous gifts from T. Neufeld, University of Minnesota, Minneapolis, MN. UAS-*Xbp1-eGFP*⁴⁵ and UAS-*ninaE*^{G69D} are generous gifts from H. Steller, The Rockefeller University, New York, NY. *Mef2-GAL4*, *r4-GAL4*, and *da-GAL4* (BDSC) transposon-containing stocks were used for muscle-specific, fat body-specific, and ubiquitous expression of RNAi constructs or transgenes. The *c754-GAL4 hsFLP*; *FRT*^{G13} UAS-*mCD8GFP* and *FRT*^{G13} *ttv*⁰⁰⁶⁸¹/*CyOGFP* strains were generated using stocks obtained from the BDSC.

When starvation was involved in an experimental procedure, third instar larvae were removed from food media and placed on filter paper soaked with 20% sucrose (Mallinckrodt Chemicals, 8360–06) solution in Petri dishes for 3 h before dissection. Fed control larvae were maintained in food media until dissection.

Real-time quantitative polymerase chain reaction

Total RNA was extracted from whole second ($n = \sim 40$) or third ($n = \sim 20$) instar larvae using NeocleoSpin RNA extraction kit (Macherey-Nagel, 740955) following the

manufacturer's manual. All genotypes were analyzed in biological triplicate. RNAi constructs were expressed ubiquitously under the control of *Da-GAL4*, and crosses were maintained at 25°C. For each sample, 0.5 mg of total RNA was used for reverse transcription of RNA in 10- μ l reaction mix using qScript cDNA SuperMix (Quanta Biosciences, 95048) to generate first strand cDNA. Real-time quantitative PCR was performed using the Perfecta™ SYBR® Green Supermix, ROX™ (Quanta Biosciences, 95055) on StepOnePlus™ (Applied Biosystems). Primers used: *sfl*: forward TCCCGCACCCAT-TATCAAC, reverse TCAAACACAATCACGCCATAAC; *ttv*: forward ATCCCGCTCTTCCACAAAC, reverse GTCGTA-TCTGTCGTATTCCCG; *Atg5*: forward GCACGCACGG-CATTGATCTACA, reverse GCCCTGGGATTTGCTGGAAT; *Atg7*: forward TTTTGCCTCACTCCATCCGTGG, reverse ATCCTCGTCGCTATCGGACATG; *Atg8a*: forward CAAC-CAACCAACCAACTTTCC, reverse GCATTCGCACGGAT-CAATTAC; *RpL32*: forward GCAAGCCCAAGGGTATCGA, reverse ACCGATGTTGGGCATCAGA. The relative RNA levels of each sample were found by comparing the amplification of the gene(s) of interest first to the internal control gene *RpL32*, and then calculating the relative change in comparison to a likewise internally corrected value from the genotypic control.

Immunohistochemistry and lysotracker red staining

Wandering third instar larvae were dissected in ice-cold Ca²⁺ free HL-3 medium (70 mM NaCl, 5 mM KCl, 20 mM MgCl₂, 10 mM NaHCO₃, 5 mM trehalose [Alfa Aesar, A19434], 100 mM sucrose, 5 mM HEPES, pH 7.2). Samples were fixed in 4% paraformaldehyde for 30 min (except samples for anti-HS antibody staining), followed by intensive washing with phosphate-buffered saline (PBS: 137 mM NaCl, 2.7 mM KCl, 10 mM Na₂HPO₄, 1.8 mM KH₂HPO₄, pH 7.4). Muscle preparations with no trace of fixative solution left were blocked in 10% normal goat serum (MP Bio-medicals, IC642921) for 1 h at room temperature and then incubated with primary antibodies for at least 12 h at 4°C. Samples were intensively washed with PBST (PBS plus .1% Triton X-100 [IBI Scientific, IB07100]) and incubated with secondary antibody for 1 h at room temperature. Muscle preparations were then washed as before and incubated overnight in mounting media before being mounted on glass slides. Primary antibodies were used at following concentrations: goat anti-HRP antibody (1:1000, conjugated with Alexa fluor 488; Jackson ImmunoResearch Laboratories, 123-545-021), anti-ubiquitin antibody (1:1000, FK2; Enzo, BML-PW8810-0100), anti-ref(2)P²⁶ (1:5000) and anti-mitochondria antibody (1:500, 4C7; Developmental Studies Hybridoma Bank, 4C7). Alexa Fluor fluorescence-conjugated secondary antibodies (1:1000) were obtained from Life Technologies (A21070, A21050, A11003, A11010, A11001, A11008).

For heparan sulfate staining, body-wall muscle preparations were fixed in Bouin fixative (70% picric acid, 25% formaldehyde [37%], 5% glacial acetic acid) for 80 min, quenched with 0.5% H₂O₂ for 1 h, and treated with 20 mU heparitinase I (Seikagaku, 100704) in heparitinase I buffer for 2 h at 37°C.

Samples were then incubated overnight with anti-heparan sulfate antibody (1:100, 3G10; Seikagaku, 270426) at 4°C. Signals were amplified using Tyramide Signal Amplification Fluorescence Systems (PerkinElmer, NEL744001KT). All of these procedures were performed at room temperature.

For LysoTracker Red staining in muscle cells, wandering third instar larvae were dissected in Ca²⁺-free HL-3 (70 mM NaCl, 5 mM KCl, 20 mM MgCl₂, 10 mM NaHCO₃, 5 mM trehalose, 115 mM sucrose, 5 mM HEPES, pH 7.2) and incubated with 100 nM LysoTracker Red DND-99 (Life Technologies, L-7528) for 5 min in the absence of light, rinsed twice with PBS, and imaged immediately. All of these procedures were performed at room temperature.

For LysoTracker Red staining in fat body cells, fed or starved third instar larvae were dissected in PBS. Fat bodies were incubated in 100 nM LysoTracker Red DND-99, 1 μ M Hoechst 33342 (Life Technologies, H3570) in PBS for 2 min. Fat bodies were then rinsed twice with PBS, transferred to 40% glycerol on glass slides, covered, and imaged immediately. All of these procedures were performed at room temperature.

Mosaic analysis

c754-GAL4 hsFLP; FRT^{G13} UAS-mCD8-GFP virgin females were mated with *FRT^{G13} ttv⁰⁰⁶⁸¹/CyOGFP* males. Eggs were collected in yeast paste on grape juice agar (2.2% agar, 1.2% sucrose, 25% grape juice concentrate) plates for 6 h, immediately followed by a 1-h heat shock at 37°C. The eggs were allowed to recover overnight at 25°C before being transferred to food medium. Larvae were reared at 25°C on instant food medium under a 12 h light/dark cycle. Feeding stage 3rd instar larvae were picked out of the food media and sorted by gender, discarding the females. Male larvae bearing the *CyOGFP* balancer were identified by strong GFP fluorescence in the testes and discarded. The remaining male larvae exhibiting GFP fluorescence in the pattern directed by *c754-GAL4>UAS-mCD8GFP* only were dissected and stained with LysoTracker Red as described above. Homozygous mutant clones were identified by loss of the *mCD8GFP* marker.

Image acquisition and analysis

Images were acquired at room temperature using an Olympus Fluoview FV1000 laser-scanning confocal microscope (Olympus America, Waltham, MA, USA). FV10-ASW 2.1 software (Olympus, Waltham, MA, USA) was used to capture images. When more than one fluorophore was detected, sequential line scanning was performed to avoid spectral bleed through artifacts. Images of samples with different genotypes within a single experiment were captured, processed, and analyzed using the same settings. Images were presented as Z-stacks of maximum intensity projections using Imaris 7.3 software (Bitplane Inc.). Three-dimensional surface reconstructions were generated from serial images taken by confocal microscopy using Imaris 7.3. The numbers of or area covered by GFP-Atg8a, GFP-mcherry-Atg8a, ref(2)P, ubiquitin, and LysoTracker Red-positive signals were measured using ImageJ1.42q. The absolute values from each animal were individually normalized by muscle size/tissue area. Adobe Photoshop CS5 (Adobe

Systems Inc.) was then used to crop images and adjust brightness and contrast. All adjustments to contrast and brightness made to ease interpretation of confocal images were applied identically to all genotypes within the experiment.

Western blot

Ubiquitous expression of both UAS-GFP-ref(2)P (GFP-ref[2]P) together with RNAi or overexpression constructs was directed by *da-GAL4*. Larvae were reared at 25°C. Five wandering 3rd instar larvae were homogenized by plastic pestle in 200 μ l ice cold protein extraction buffer (20 mM HEPES, 100 mM KCl, 10 mM EDTA, 1 mM DTT, .1% Triton X-100, 5% glycerol, 1X protease inhibitor cocktail Complete [Roche, 10184600])⁷⁷ for each genotype. Samples were centrifuged for 10 min, and the supernatant was removed to a clean tube. Protein concentration was measured by BCA Protein Assay (Pierce, 23227), and samples were diluted to a standard concentration using 4x protein loading buffer⁷⁸ and protein extraction buffer, then boiled at 95°C for 5 min. Approximately 25 μ g total protein per sample was run on an 8% polyacrylamide gel. After transfer, the nitrocellulose membrane was rinsed in TBS (50 mM Tris-Cl, 150 mM NaCl, pH 7.6) and dried overnight. The membrane was rehydrated and blocked in 0.5% TBST (TBS plus 0.5% Tween 20 [BDH, 4210])⁷⁹ and incubated overnight at 4°C with rabbit polyclonal anti-GFP (1:1500, CAB3211; Thermo Scientific, CAB4211). Goat anti-rabbit-HRP secondary antibody was applied at 1:3000 (Invitrogen, 31430). ECL detection was performed using G:BOX Chemi XG4 (Syngene, Frederick, MD, USA) which was also used to invert coloration of resulting images. Band signal density was assessed using ImageJ1.42q.

Assessment of UAS-mito-GFP phenotypes

Confocal images taken from animals bearing no RNAi expression construct were carefully examined and analyzed based on visible features. A summary of common features and the scope of variation seen in those features between images was generated by assessing the fluorescent intensity of the *mito-GFP* reporter, the mitochondrial shapes, sizes, and density within each animal. The summaries of these 4 features were then used as a qualitative standard for what constitutes a normal mitochondrial phenotype as observed by *mito-GFP*. The confocal images from all animals, including these wild-type controls, were then blinded by replacing the image identifier with a randomly generated number (nonrepeating integer sequence generated by random.org) and scored as ‘normal’ or ‘substantially abnormal’ based on comparison to the qualitative standard of normality. The scored images were then unblinded and the results were assembled into a contingency table.

Transmission electron microscopy

Wandering third instar larvae were dissected in ice-cold Ca²⁺-free HL-3 medium and fixed overnight with TEM fixative solution (1.5% glutaraldehyde, 2.5% paraformaldehyde, 1.8 mM Ca²⁺ in 0.1 M sodium-cacodylate buffer, pH 7.0) at 4°C. Post-fixation (1% osmium tetroxide in 0.1 M sodium-cacodylate

buffer, pH 7.0) and en bloc staining (2% uranyl acetate) were performed in a dark container for 2 h each. Samples were washed with 0.1 M sodium cacodylate buffer (pH 7.4) between fixations and before staining. Muscle preparations were then dehydrated (gradient ethanol range from 50% to 100%, 100% acetone, 70 min in total) and infiltrated (1:1 acetone:resin, 1:3 acetone:resin, 100% resin, 2 d in total). Samples were embedded in Spurr’s low viscosity resin (Electron Microscopy Sciences, 14300) at 60°C for ~60 h, allowing for polymerization. The sample cubes were sectioned to thin (~70 nm) slices and images were obtained with a JEOL1200 transmission electron microscope (Peabody, MA, USA) and analyzed by ImageJ1.42q.

The measurement of membrane content provided a way to assess the density of SSR. It was calculated as the area of the electron dense membrane bilayers divided by the total area encompassed by the SSR (with the motoneuron terminal area subtracted out). The number of autophagosomes was counted manually and the values were normalized by muscle area for each graph. Mitochondrial density was determined as the area of electron dense mitochondria divided by the total area of muscle surface.

Statistical analysis

Statistical analyses for quantitative data were performed with Minitab Release 16 (Minitab). All data points were presented as mean \pm SEM. Normality of data distribution was determined using probability plots. Comparisons between 2 groups were performed using the Student *t* test for normally distributed data or Mann-Whitney test for nonparametric data. Comparisons between more than 2 groups were performed using ANOVA for normally distributed data or Kruskal-Wallis for nonparametric data, followed by the Tukey test or Mann-Whitney test. When analyzing the contingency table of mitochondrial morphology, expected values for occurrence of an abnormal score were often less than 5 so pairwise comparisons were performed using the Fisher exact test.

Abbreviations

Atg5	autophagy-related 5
Atg7	autophagy-related 7
Atg8a	autophagy-related 8a
botv	brother of tout-velu (<i>Drosophila</i> EXT3 homolog)
ER	endoplasmic reticulum
Ext2	exostosin glycosyltransferase 2
HS	heparan sulfate
HSPG	heparan sulfate proteoglycan
mCD8-GFP	Mus musculus CD8 protein fused with green fluorescent protein
MSD	multiple sulfatase deficiency
NMJ	neuromuscular junction
Pi3K92E	phosphatidylinositol 3-kinase class I (<i>Drosophila</i> gene)
PI3K	class I phosphatidylinositol 3-kinase, species nonspecific
QPCR	quantitative polymerase chain reaction

ref(2)P	refractory to sigma P (<i>Drosophila</i> SQSTM1 homolog)
SUMF1	sulfatase modifying factor 1 (Homo sapiens)
Sumf1	sulfatase modifying factor 1 (Mus musculus)
SSR	subs synaptic reticulum
sfl	sulfateless (<i>Drosophila</i> N-deacetylase N-sulfotransferase)
TEM	transmission electron microscopy
TOR	target of rapamycin (MTOR in mammalian species)
ttv	tout-velu (<i>Drosophila</i> EXT1 homolog)
w	white

Disclosure of potential conflicts of interest

No potential conflicts of interest were disclosed.

Acknowledgments

We are grateful to Thomas Neufeld, Hermann Steller, the Bloomington *Drosophila* stock center and the Vienna *Drosophila* RNAi Center for fly stocks. We are grateful to Richard Ordway for sharing the ref(2)P antibody. We also acknowledge the Microscopy and Cytometry Facility at The Pennsylvania State University for technical assistance with electron microscopy.

Funding

This work was supported by National Institutes of Health grant 5 R01 GM054832–15 and funds to SBS from The Pennsylvania State University.

References

- Lin X. Functions of heparan sulfate proteoglycans in cell signaling during development. *Development* 2004; 131:6009–21; PMID:15563523; <https://doi.org/10.1242/dev.01522>
- Lander AD, Selleck SB. The elusive functions of proteoglycans: in vivo veritas. *J Cell Biol* 2000; 148:227–32; PMID:10648554; <https://doi.org/10.1083/jcb.148.2.227>
- Bishop JR, Schuksz M, Esko JD. Heparan sulphate proteoglycans fine-tune mammalian physiology. *Nature* 2007; 446:1030–7; PMID:17460664; <https://doi.org/10.1038/nature05817>
- Hacker U, Nybakken K, Perrimon N. Heparan sulphate proteoglycans: the sweet side of development. *Nat Rev Mol Cell Biol* 2005; 6:530–41; PMID:16072037; <https://doi.org/10.1038/nrm1681>
- Kirkpatrick CA, Selleck SB. Heparan sulfate proteoglycans at a glance. *J Cell Sci* 2007; 120:1829–32; PMID:17515480; <https://doi.org/10.1242/jcs.03432>
- Sarrazin S, Lamanna WC, Esko JD. Heparan sulfate proteoglycans. *Cold Spring Harb Perspect Biol* 2011; 3:a004952; PMID:21690215; <https://doi.org/10.1101/cshperspect.a004952>
- Selleck SB. Proteoglycans and pattern formation: sugar biochemistry meets developmental genetics. *Trends Genet* 2000; 16:206–12; PMID:10782114; [https://doi.org/10.1016/S0168-9525\(00\)01997-1](https://doi.org/10.1016/S0168-9525(00)01997-1)
- Johnson KG, Tenney AP, Ghose A, Duckworth AM, Higashi ME, Parfitt K, Marcu O, Heslip TR, Marsh JL, Schwarz TL, et al. The HSPGs syndecan and dallylike bind the receptor phosphatase LAR and exert distinct effects on synaptic development. *Neuron* 2006; 49:517–31; PMID:16476662; <https://doi.org/10.1016/j.neuron.2006.01.026>
- Stryker E, Johnson KG. LAR, liprin alpha and the regulation of active zone morphogenesis. *J Cell Sci* 2007; 120:3723–8; PMID:17959628; <https://doi.org/10.1242/jcs.03491>
- Kamimura K, Ueno K, Nakagawa J, Hamada R, Saitoe M, Maeda N. Perlecan regulates bidirectional Wnt signaling at the *Drosophila* neuromuscular junction. *J Cell Biol* 2013; 200:219–33; PMID:23319599; <https://doi.org/10.1083/jcb.201207036>
- Ren Y, Kirkpatrick CA, Rawson JM, Sun M, Selleck SB. Cell type-specific requirements for heparan sulfate biosynthesis at the *Drosophila* neuromuscular junction: Effects on synapse function, membrane trafficking, and mitochondrial localization. *J Neurosci* 2009; 29:8539–50; PMID:19571145; <https://doi.org/10.1523/JNEUROSCI.5587-08.2009>
- Bellaiche Y, The I, Perrimon N. Tout-velu is a *Drosophila* homologue of the putative tumour suppressor EXT-1 and is needed for Hh diffusion. *Nature* 1998; 394:85–8; PMID:9665133; <https://doi.org/10.1038/27932>
- Duffy JB. GAL4 system in *Drosophila*: a fly geneticist's Swiss army knife. *Genesis* 2002; 34:1–15; PMID:12324939; <https://doi.org/10.1002/gene.10150>
- Han C, Belenkaya TY, Khodoun M, Tauchi M, Lin X, Lin X. Distinct and collaborative roles of *Drosophila* EXT family proteins in morphogen signalling and gradient formation. *Development* 2004; 131:1563–75; PMID:14998928; <https://doi.org/10.1242/dev.01051>
- Lin H, Huber R, Schlessinger D, Morin PJ. Frequent silencing of the GPC3 gene in ovarian cancer cell lines. *Cancer Res* 1999; 59:807–10; PMID:10029067
- Toyoda H, Kinoshita-Toyoda A, Fox B, Selleck SB. Structural analysis of glycosaminoglycans in animals bearing mutations in sugarless, sulfateless, and tout-velu. *Drosophila* homologues of vertebrate genes encoding glycosaminoglycan biosynthetic enzymes. *J Biol Chem* 2000; 275:21856–61; PMID:10806213; <https://doi.org/10.1074/jbc.M003540200>
- Toyoda H, Kinoshita-Toyoda A, Selleck SB. Structural analysis of glycosaminoglycans in *Drosophila* and *Caenorhabditis elegans* and demonstration that tout-velu, a *Drosophila* gene related to EXT tumor suppressors, affects heparan sulfate in vivo. *J Biol Chem* 2000; 275:2269–75; PMID:10644674; <https://doi.org/10.1074/jbc.275.4.2269>
- Schmid A, Chiba A, Doe CQ. Clonal analysis of *Drosophila* embryonic neuroblasts: neural cell types, axon projections and muscle targets. *Development* 1999; 126:4653–89; PMID:10518486
- Atwood HL, Govind CK, Wu CF. Differential ultrastructure of synaptic terminals on ventral longitudinal abdominal muscles in *Drosophila* larvae. *J Neurobiol* 1993; 24:1008–24; PMID:8409966; <https://doi.org/10.1002/neu.480240803>
- Gorczyca M, Popova E, Jia XX, Budnik V. The gene mod(mdg4) affects synapse specificity and structure in *Drosophila*. *J Neurobiol* 1999; 39:447–60; PMID:10363916; [https://doi.org/10.1002/\(SICI\)1097-4695\(19990605\)39:3%3c447::AID-NEU10%3e3.0.CO;2-Q](https://doi.org/10.1002/(SICI)1097-4695(19990605)39:3%3c447::AID-NEU10%3e3.0.CO;2-Q)
- Teodoro RO, Pekkurnaz G, Nasser A, Higashi-Kovtun ME, Balakireva M, McLachlan IG, Camonis J, Schwarz TL. Ral mediates activity-dependent growth of postsynaptic membranes via recruitment of the exocyst. *EMBO J* 2013; 32:2039–55; PMID:23812009; <https://doi.org/10.1038/emboj.2013.147>
- Gorczyca D, Ashley J, Speese S, Gherbesi N, Thomas U, Gundelfinger E, Gramates LS, Budnik V. Postsynaptic membrane addition depends on the Discs-Large-interacting t-SNARE Gtaxin. *J Neurosci* 2007; 27:1033–44; PMID:17267557; <https://doi.org/10.1523/JNEUROSCI.3160-06.2007>
- Lee HG, Zhao N, Campion BK, Nguyen MM, Selleck SB. Akt regulates glutamate receptor trafficking and postsynaptic membrane elaboration at the *Drosophila* neuromuscular junction. *Dev Neurobiol* 2013; 73:723–43; PMID:23592328; <https://doi.org/10.1002/dneu.22086>
- Hailey DW, Rambold AS, Satpute-Krishnan P, Mitra K, Sougrat R, Kim PK, Lippincott-Schwartz J. Mitochondria supply membranes for autophagosome biogenesis during starvation. *Cell* 2010; 141:656–67; PMID:20478256; <https://doi.org/10.1016/j.cell.2010.04.009>
- Klionsky DJ. Autophagy: from phenomenology to molecular understanding in less than a decade. *Nat Rev Mol Cell Biol* 2007; 8:931–7; PMID:17712358; <https://doi.org/10.1038/nrm2245>
- Pircs K, Nagy P, Varga A, Venkei Z, Erdi B, Hegedus K, Juhasz G. Advantages and limitations of different p62-based assays for

- [59] Cosma MP, Pepe S, Annunziata I, Newbold RF, Grompe M, Parenti G, Ballabio A. The multiple sulfatase deficiency gene encodes an essential and limiting factor for the activity of sulfatases. *Cell* 2003; 113:445-56; PMID:12757706; [https://doi.org/10.1016/S0092-8674\(03\)00348-9](https://doi.org/10.1016/S0092-8674(03)00348-9)
- [60] Dierks T, Schmidt B, Borissenko LV, Peng J, Preusser A, Mariappan M, von Figura K. Multiple sulfatase deficiency is caused by mutations in the gene encoding the human C(alpha)-formylglycine generating enzyme. *Cell* 2003; 113:435-44; PMID:12757705; [https://doi.org/10.1016/S0092-8674\(03\)00347-7](https://doi.org/10.1016/S0092-8674(03)00347-7)
- [61] Settembre C, Arteaga-Solis E, McKee MD, de Pablo R, Al Awqati Q, Ballabio A, Karsenty G. Proteoglycan desulfation determines the efficiency of chondrocyte autophagy and the extent of FGF signaling during endochondral ossification. *Genes Dev* 2008; 22:2645-50; <https://doi.org/10.1101/gad.1711308>
- [62] Settembre C, Fraldi A, Jahreiss L, Spampanato C, Venturi C, Medina D, de Pablo R, Tacchetti C, Rubinsztein DC, Ballabio A. A block of autophagy in lysosomal storage disorders. *Hum Mol Genet* 2008; 17:119-29; PMID:17913701; <https://doi.org/10.1093/hmg/ddm289>
- [63] Settembre C, Fraldi A, Rubinsztein DC, Ballabio A. Lysosomal storage diseases as disorders of autophagy. *Autophagy* 2008; 4:113-4; PMID:18000397; <https://doi.org/10.4161/auto.5227>
- [64] Settembre C, Arteaga-Solis E, Ballabio A, Karsenty G. Self-eating in skeletal development: implications for lysosomal storage disorders. *Autophagy* 2009; 5:228-9; PMID:19029806; <https://doi.org/10.4161/auto.5.2.7390>
- [65] Annunziata I, Bouche V, Lombardi A, Settembre C, Ballabio A. Multiple sulfatase deficiency is due to hypomorphic mutations of the SUMF1 gene. *Hum Mutat* 2007; 28:928; PMID:17657823; <https://doi.org/10.1002/humu.9504>
- [66] Abid MR, Guo S, Minami T, Spokes KC, Ueki K, Skurk C, Walsh K, Aird WC. Vascular endothelial growth factor activates PI3K/Akt/forkhead signaling in endothelial cells. *Arterioscler Thromb Vasc Biol* 2004; 24:294-300; PMID:14656735; <https://doi.org/10.1161/01.ATV.0000110502.10593.06>
- [67] Dey JH, Bianchi F, Voshol J, Bonenfant D, Oakeley EJ, Hynes NE. Targeting fibroblast growth factor receptors blocks PI3K/AKT signaling, induces apoptosis, and impairs mammary tumor outgrowth and metastasis. *Cancer Res* 2010; 70:4151-62; PMID:20460524; <https://doi.org/10.1158/0008-5472.CAN-09-4479>
- [68] Berry DL, Baehrecke EH. Growth arrest and autophagy are required for salivary gland cell degradation in *Drosophila*. *Cell* 2007; 131:1137-48; PMID:18083103; <https://doi.org/10.1016/j.cell.2007.10.048>
- [69] Rusten TE, Lindmo K, Juhasz G, Sass M, Seglen PO, Brech A, Stenmark H. Programmed autophagy in the *Drosophila* fat body is induced by ecdysone through regulation of the PI3K pathway. *Dev Cell* 2004; 7:179-92; PMID:15296715; <https://doi.org/10.1016/j.devcel.2004.07.005>
- [70] Tang G, Gudsnuk K, Kuo SH, Cotrina ML, Rosoklija G, Sosunov A, Sonders MS, Kanter E, Castagna C, Yamamoto A, et al. Loss of mTOR-dependent macroautophagy causes autistic-like synaptic pruning deficits. *Neuron* 2014; 83:1131-43; PMID:25155956; <https://doi.org/10.1016/j.neuron.2014.07.040>
- [71] Shen W, Ganetzky B. Autophagy promotes synapse development in *Drosophila*. *J Cell Biol* 2009; 187:71-9; PMID:19786572; <https://doi.org/10.1083/jcb.200907109>
- [72] Rowland AM, Richmond JE, Olsen JG, Hall DH, Bamber BA. Pre-synaptic terminals independently regulate synaptic clustering and autophagy of GABAA receptors in *Caenorhabditis elegans*. *J Neurosci* 2006; 26:1711-20; <https://doi.org/10.1523/JNEUROSCI.2279-05.2006>
- [73] Dietzl G, Chen D, Schnorrer F, Su KC, Barinova Y, Fellner M, Gasser B, Kinsey K, Oppel S, Scheiblauer S, et al. A genome-wide transgenic RNAi library for conditional gene inactivation in *Drosophila*. *Nature* 2007; 448:151-6; PMID:17625558; <https://doi.org/10.1038/nature05954>
- [74] Perkins LA, Holderbaum L, Tao R, Hu Y, Sopko R, McCall K, Yang-Zhou D, Flockhart I, Binari R, Shim HS, et al. The Transgenic RNAi Project at Harvard Medical School: Resources and Validation. *Genetics* 2015; 201:843-52; PMID:26320097; <https://doi.org/10.1534/genetics.115.180208>
- [75] Juhasz G, Hill JH, Yan Y, Sass M, Baehrecke EH, Backer JM, Neufeld TP. The class III PI(3)K Vps34 promotes autophagy and endocytosis but not TOR signaling in *Drosophila*. *J Cell Biol* 2008; 181:655-66; PMID:18474623; <https://doi.org/10.1083/jcb.200712051>
- [76] Chang YY, Neufeld TP. An Atg1/Atg13 complex with multiple roles in TOR-mediated autophagy regulation. *Mol Biol Cell* 2009; 20:2004-14; PMID:19225150; <https://doi.org/10.1091/mbc.E08-12-1250>
- [77] Emery P. Protein extraction from *Drosophila* heads. *Methods Mol Biol* 2007; 362:375-7; PMID:17417024
- [78] Cumming RC, Simonsen A, Finley KD. Quantitative analysis of autophagic activity in *Drosophila* neural tissues by measuring the turnover rates of pathway substrates. *Methods Enzymol* 2008; 451:639-51; PMID:19185743
- [79] Batteiger B, Newhall WJt, Jones RB. The use of Tween 20 as a blocking agent in the immunological detection of proteins transferred to nitrocellulose membranes. *J Immunol Methods* 1982; 55:297-307; PMID:6820029; [https://doi.org/10.1016/0022-1759\(82\)90089-8](https://doi.org/10.1016/0022-1759(82)90089-8)